A phenomenological model for bubble coalescence in confined highly porous media

Marion Serres [a,b], Timothée Maison [a], Régis Philippe [b], Valérie Vidal [a,*]

[a] *Laboratoire de Physique, CNRS UMR 5672, École Normale Supérieure de Lyon, Université de Lyon, 46 Allée d'Italie, Lyon 69007, France*
[b] *Laboratoire de Génie des Procédés Catalytiques, CNRS UMR 5285, CPE Lyon, Université de Lyon, 43 Boulevard du 11 Novembre 1918, Villeurbanne 69100, France*

ABSTRACT

In a recent work, Serres et al. (2016) considered the stability of Taylor bubbles entering a confined highly porous medium (open cell solid foam of 96% porosity). This experimental work pointed out that a periodic alternation of gas bubbles and liquid slugs in a millichannel can either keep its regularity, or be destructured at the porous medium entrance. A critical bubble length was proposed as a transition parameter between the two observed regimes. This study presents two key results which complement the previous work and explain the regime transition. (1) The comparison of the Taylor flow upstream the porous medium with the Taylor flow in an empty millichannel demonstrates that the regime transition is not due to the possible feedback of the foam on the upstream flow. (2) A phenomenological model is proposed, which accounts for the observed bubble coalescence and gas channelling in the porous medium in the range of parameters explored in the experiments.

© 2018 Elsevier Ltd. All rights reserved.

1. Introduction

Three-phase flows are ubiquitous in a wide range of phenomena, from natural to industrial processes. In the last decades, gas-liquid flows in porous media – either rigid or mobile – have motivated many fundamental and applied studies, with the goal to either understand and predict natural processes such as methane venting (Naudts et al., 2008) and pockmarks (Hovland et al., 2002; Gay et al., 2006) on the oceanic floor or mud volcanoes (Planke et al., 2003; Mastalerz et al., 2007; Mazzini et al., 2007), or to optimize man-made techniques. Among these latters, soil decontamination by air sparging (Semer et al., 1998; Reddy and Adams, 2001), CO_2 sequestration (Kang et al., 2005; Eccles et al., 2009) enhanced oil recovery (Babchin et al., 2008) or catalytic reactors (Losey et al., 2001; Hessel et al., 2005; Marquez et al., 2008) are part of the present societal challenges. Indeed, the strong hydrodynamic coupling between the gas, liquid and – in mobile porous media – solid phase motion, in addition to possible mixing and chemical reactions, make this problem very difficult to tackle.

In the particular context of heterogeneous catalysis, process intensification has led to testing new porous materials and environments. In confined geometries, open cell solid foams are innovative porous media which have a great potential due to their high porosity (up to 96%), leading to low pressure losses, large contact area and possibly enhanced mass and heat transfer (Stemmet et al., 2005; 2006; 2008; Twigg and Richardson, 2007; Tourvielle et al., 2015a; 2015b; Lali et al., 2016; Zapico et al., 2016). However, if the interest of such new material has been undoubtfully highlighted, the hydrodynamics of a confined gas-liquid flow across such medium still has to be characterized.

In a recent work, Serres et al. (2016) have quantified the local hydrodynamics of a periodic gas-liquid flow – Taylor flow – forced into an open cell solid foam in a confined geometry (horizontal square millichannel). They have shown that, in a given range of parameters, the periodic flow in the millichannel disorganizes at the porous medium entrance, leading to a modulation of the upstream Taylor flow frequency. The transition was successfully described in terms of a modified Weber number (see Serres et al. (2016) and Section 3.2 of the present work). A tentative model was proposed in terms of bubble fragmentation at the foam entrance, but without any further quantification.

In the present study, we revisit the work of Serres et al. (2016) based on new experimental evidences. First, we demonstrate that the Taylor frequency upstream can be predicted by a simple model of the periodic gas-liquid flow (Section 3.1). It demonstrates that the existence of the modulated regime is not due to a change in the upstream flow, but rather to the presence of the porous medium. We then propose a phenomenological model (Section 4) based on bubble coalescence and gas channelling – as
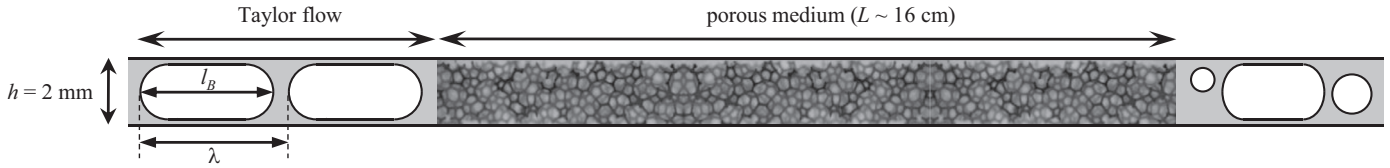
Fig. 1. Sketch of the experimental setup. Periodic gas bubbles and liquid slugs (Taylor flow) are sent at the entrance of a porous medium of length $L \sim 16$ cm in a millichannel of square cross-section $h = 2$ mm. l_B is the typical bubble length and λ the spatial periodicity of the Taylor flow.

evidenced by new experimental measurements. This model successfully describes the transition between the periodic, Taylor-like regime and the modulated regime.

2. Preliminary results

2.1. Experimental setup

The experimental setup is a millichannel of square cross-section $h \times h$ ($h = 2$ mm). The setup is similar to the one presented in Serres et al. (2016), and therefore is only briefly described here. A regular Taylor flow, consisting of a periodic alternance of gas bubbles and liquid slugs (Garstecki et al., 2006; Angeli and Gavriilidis, 2008), is sent at the entrance of a porous medium of length $L \simeq 16$ cm (Fig. 1). This latter consists of a highly porous structure, an open cell solid foam made of vitreous carbon (80 PPI, ERG Aerospace, porosity $\epsilon = 96\%$). The pore size distribution is characterized by X-Ray tomography (GE Phoenix v|tome|x s, RX tube of 160kV with focal point of up to 1 μm) with a spatial resolution of 5 μm. It evidences two pore structures: (1) the cells, corresponding to the void cages of the foam and (2) the windows, which connect two neighboring cells (for more details, see Serres et al., 2016). The typical diameter of the cells and windows are $d_c = 604 \pm 86$ μm and $d_w = 257 \pm 85$ μm, respectively.

The gas (G) and liquid (L) are nitrogen and ethanol of density $\rho_G = 1.25$ kg/m^3, $\rho_L = 795$ kg/m^3, viscosity $\mu_G = 1.76 \times 10^{-5}$ Pa s, $\mu_L = 1.15 \times 10^{-3}$ Pa s and $\sigma \simeq 22$ mN/m, the nitrogen-ethanol surface tension at room temperature (Dittmar et al., 2003). The flow-rates are varied as follows, $Q_G = [2 - 35]$ Ncm^3 min^{-1} and $Q_L = [0.5 - 8]$ Ncm^3 min^{-1}, such that their ratio stays in the range $Q_G/Q_L = [0.25 - 35]$, ensuring a regular Taylor flow upstream the porous medium.

One of the experimental cell wall is made of glass, and makes it possible to visualize directly the gas-liquid flow in the millichannel. A fluorescent dye (Rhodamine 6B, 3.2×10^{-5} mol/L) is dissolved inside the liquid phase (ethanol) prior to the injection, ensuring a good contrast between the liquid (bright gray) and the gas (black) phases on the images (Fig. 2a). The experimental data of gas and liquid flow with a porous medium were reanalyzed from Serres et al. (2016), for which images acquisition was performed with a camera Solinocam H2D2 at 113 frames per second mounted on a fluorescence microscope Olympus BX51M. To get a better insight on the gas and liquid flow, additional images acquisition was performed with a fast camera (Optronis CR 600 × 2 at 1000 fps). These experiments made it possible to observe the flow dynamics inside the porous medium (see end of Section 3) and quantify the relevant ingredients for the phenomenological model (Section 4). Finally, similar experiments in an empty channel (without porous medium) were also performed in order to quantify the possible feedback of the porous medium on the upstream Taylor flow.

2.2. Data processing

After a simple normalization by a reference image and binarization process (Serres et al., 2016), the gas and liquid phases are separated in the raw images (Fig. 2a) and we extract for each
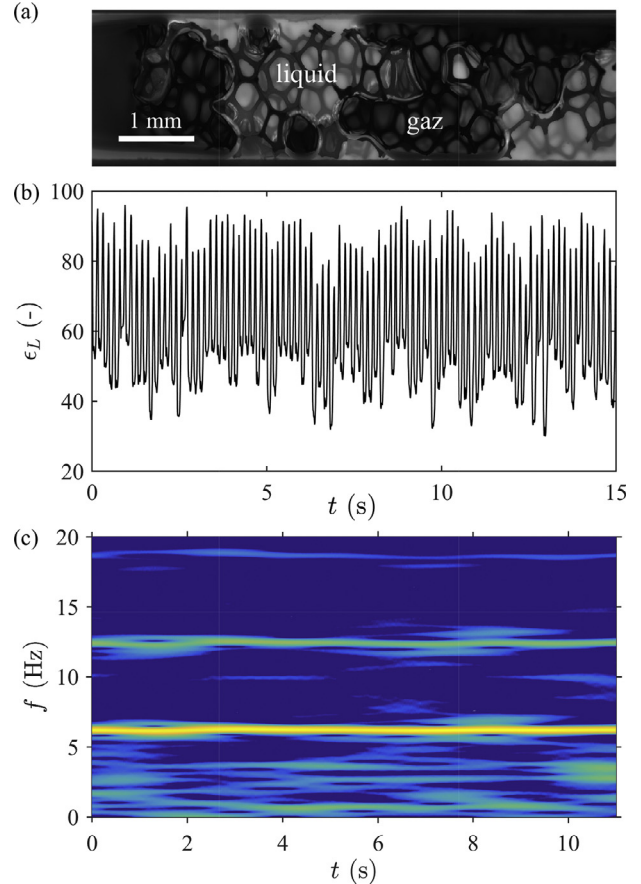

Fig. 2. Data processing [example for $Q_G = 6$ Ncm^3 min^{-1}, $Q_L = 4$ Ncm^3 min^{-1} at the entrance of the porous medium]. (a) Raw image. The gas (dark zones) and liquid (light gray zones) phases are clearly visible, as well as the foam structure. (b) Example of ϵ_L vs. t. (c) Spectrogram associated with (b), computed with a sliding window of width $\Delta t = 4$ s. The main frequency here is $f_0 \simeq 6$ Hz.

image the volume fraction of liquid, ϵ_L. This technique has been previously used in micropacked beds, where it provided a visualization of the flow close to the observed surface (Faridkhou and Larachi, 2012). In open cell solid foams, the high porosity makes it possible to visualize the gas phase over the whole channel depth. It thus provides a good estimation of the local liquid holdup, although the integration over the depth induces an underestimation of the liquid holdup due to the presence of the solid phase. Following Serres et al. (2016), ϵ_L is thus referred to as the *apparent* liquid holdup.

Fig. 2b illustrates an example of apparent liquid holdup variations in time, in which the downward peaks correspond to gas bubbles crossing the image. The frequency content of $\epsilon_L(t)$ is then quantified by means of spatiotemporal diagrams (Fig. 2c) computed with a sliding window of width $\Delta t = 4$ s. The main frequency f_0 is extracted by computing the median value of the frequency corresponding to the maximum peak in the spectrum
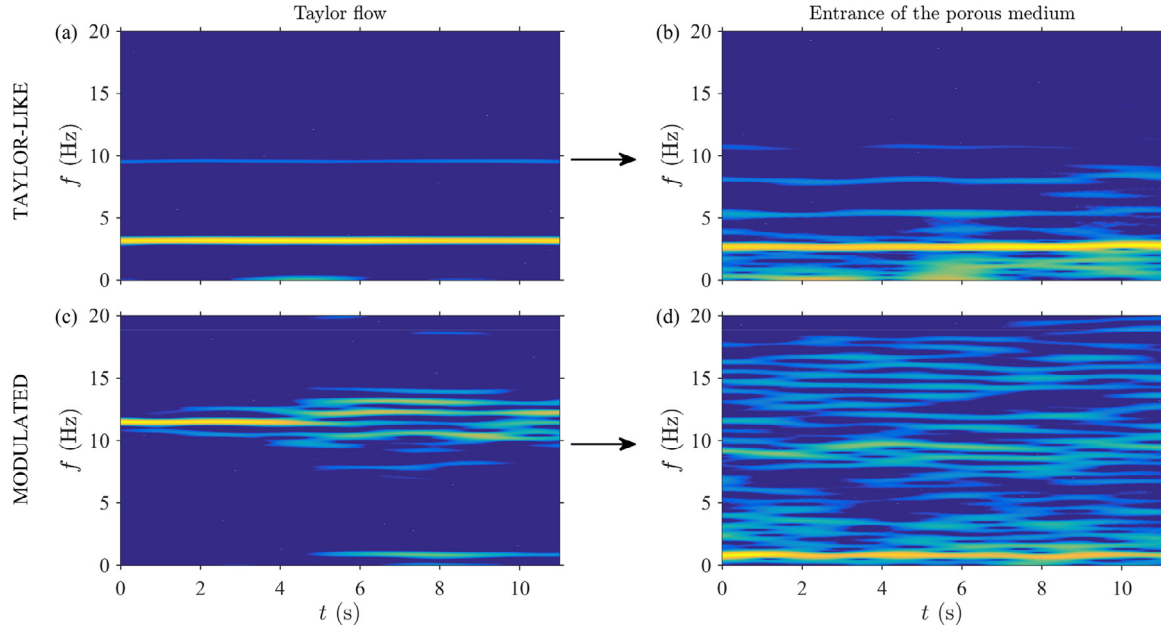
Fig. 3. Different hydrodynamic regimes. The spatiotemporal diagram of ϵ_L in the Taylor flow region, upstream the porous medium (*left column*) and at the entrance of the porous medium (*right column*) displays two different regimes. (1) The Taylor-flow frequency is not altered by the porous medium [Taylor-like regime (a,b) $Q_G = 2$ Ncm^3 min^{-1}, $Q_L = 4$ Ncm^3 min^{-1}]; (2) The Taylor flow is disorganized at the entrance of the porous medium and displays a low-frequency modulation [modulated regime (c,d) $Q_G = 10$ Ncm^3 min^{-1}, $Q_L = 4$ Ncm^3 min^{-1}]. In this last case, the disorganization by the porous medium can have a feedback on the upstream flow (see text).

at each time t, over the full acquisition (typically about 10 s). Upstream the porous medium, $f_0 = f_T$, the Taylor frequency.

2.3. Hydrodynamic regimes

The previous work of Serres et al. (2016) focused on the behavior of the Taylor bubbles when entering the porous medium. In particular, they evidenced two hydrodynamic regimes when the gas-liquid flow enters the porous medium: (1) a Taylor-like regime, for which the Taylor frequency is preserved (Fig. 3a,b); (2) a modulated regime, for which a low-frequency modulation of the initial Taylor flow periodic signal is observed (Fig. 3c,d). In this last case, we sometimes report a feedback of the low-frequency modulation on the upstream Taylor flow, as evidenced in Fig. 3c at $t \simeq 5$ s. This feedback, due to a coupling between the flow disorganization at the foam entrance and the upstream flow, is usually observed for high gas over liquid flow rates, Q_G/Q_L. In the next section, we quantify the possible disorganization of the Taylor flow at the porous medium entrance.

3. Taylor flow disorganization

3.1. Taylor flow frequency

The Taylor flow upstream the porous medium is characterized by its main frequency f_T (see Section 2.2). Here, we compare this frequency, measured experimentally, with the theoretical frequency computed as follows. In a first approximation, the relationship between the Taylor spatial wavelength λ and the bubble length l_B (see Fig. 1) is

$$\lambda \simeq l_B \left(1 + \frac{Q_L}{Q_G} \right). \qquad (1)$$

This relationship holds true as long as we neglect the lubrication films around the bubbles and consider that the liquid around the meniscii at the bubble front and rear have a negligible volume respect to the bubble volume. This latter point is always checked

experimentally. An estimation of the cross-section liquid fraction, W, in the square millichannel is provided by Leclerc et al. (2010), considering the films on the cell walls and the gutters at the four corners:

$$W = \frac{4h_L}{h}\left(1 - \frac{h_L}{h} \right) + \frac{4 - \pi}{h^2}\left(\frac{h}{4} - \frac{h_L}{2} \right)^2, \qquad (2)$$

where h is the channel width and h_L the liquid film thickness far from the channel corners. This latter can be estimated by the following relationship (Aussillous and Quéré, 2000; Roudet, 2008):

$$\frac{h_L}{h} \sim \frac{Ca^{2/3}}{1 + Ca^{2/3}} \qquad (3)$$

where $Ca = \mu U/\sigma$ is the capillary number, μ the fluid dynamic viscosity, U the typical bubble velocity and $\sigma \simeq 22$ mN/m the nitrogen-ethanol surface tension at room temperature (Dittmar et al., 2003). In all the experiments, $Ca \ll 1$ ($5.4 \times 10^{-4} < Ca < 9.7 \times 10^{-3}$), leading to $0.07 < W < 0.2$. In a first approximation, we therefore neglect the lubrication films.

As previously reported in the literature, the Taylor bubble length l_B is a linear function of the gas-liquid flow-rate ratio, Q_G/Q_L (Garstecki et al., 2006; Leclerc et al., 2010; Abadie et al., 2012; Serres et al., 2016):

$$\frac{l_B}{h} = \alpha \frac{Q_G}{Q_L} + \beta \qquad (4)$$

Fig. 4a displays the Taylor bubble length normalized by the channel width, l_B/h, as a function of the gas-liquid flow-rate ratio, Q_G/Q_L, in the experiments with the porous medium (white squares) or with the empty channel (gray stars). Both sets of data follow the linear trend expected from Eq. (4) inside the experimental error bars, computed as the standard deviation. For empty channel experiments, we report as the dashed line in Fig. 4 the linear relationship proposed by van Steijn et al. (2007) as an improvement of the Garstecki et al. (2006) model for microchannels of rectangular cross-section (Abadie et al., 2012): $\alpha = 1.5$ and $\beta = 1.5(2r/h)$ where $r = 0.5$ mm is the radius of the gas inlet, leading to $\beta =$
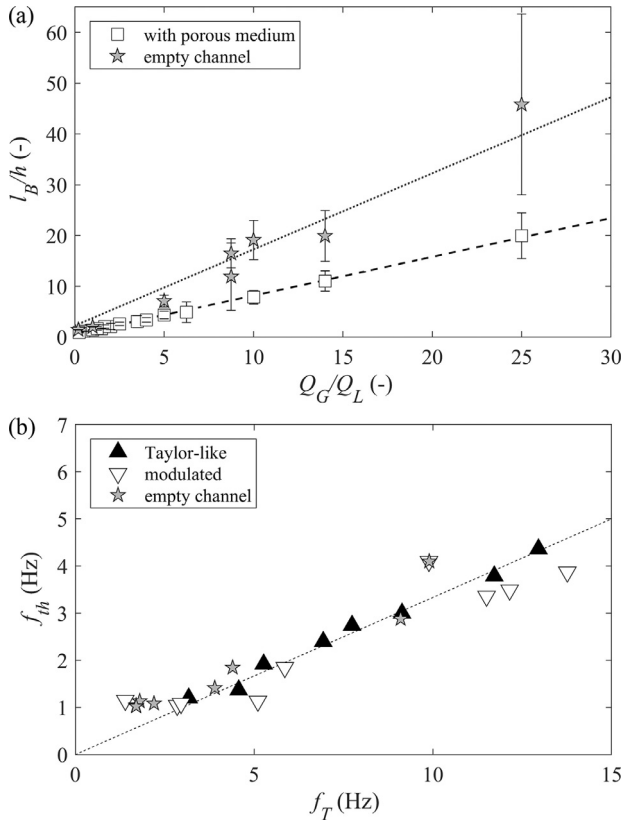
Fig. 4. (a) Normalized bubble length l_B/h as a function of the flow rates ratio Q_G/Q_L [(white squares, upstream the solid foam); (gray stars, with an empty channel)]. The lines indicate the linear relationship $l_B/h = \alpha Q_G/Q_L + \beta$ for the empty channel [$\alpha = 1.5$, $\beta = 2.25$, dotted gray line] and the bubbles upstream the porous medium [$\alpha' = 0.76$, $\beta' = 0.54$, dashed black line]. (b) Theoretical frequency of the Taylor flow f_{th} (from Eq. (5)) as a function of the Taylor bubbles frequency measured upstream the porous medium in the foam experiments, f_T [($\blacktriangle$, Taylor-like regime), ($\triangledown$, modulated regime)] and in the empty channel experiments [gray stars]. The black line is a guideline for the eyes.

2.25. Note that the error bars increase with increasing gas-liquid flow-rate ratio, as a signature of a flow becoming more irregular, and approaching the transition between a periodic Taylor flow to a churn flow (Kreutzer et al., 2005). For a same set of gas and liquid flow rates, the bubble length upstream the porous medium in the experiment with the foam is significantly lower. A linear fit gives $\alpha' = 0.76$ and $\beta' = 0.54$ (Fig. 4a, dashed line). This relation differs slightly from the one proposed in Serres et al. (2016), which only considered the rough scaling $l_B/h \simeq Q_G/Q_L$. Interestingly, although the flow through the porous medium exhibits two different hydrodynamic regimes (see Section 2.3), the bubble length upstream follows a single linear trend. This indicates that the flow dynamics inside the foam has no significant impact on the upstream flow.

The theoretical Taylor flow frequency, $f_{th} = U/\lambda$, where $U = (Q_G + Q_L)/h^2$, can be written by using λ given by Eq. (1) and l_B by Eq. (4):

$$f_{th} = \frac{Q_G + Q_L}{h^3 \left[(\alpha + \beta) + \alpha \frac{Q_G}{Q_L} + \beta \frac{Q_L}{Q_G} \right]} \qquad (5)$$

It is estimated by taking the coefficient (α, β) from the empty channel experiment. Fig. 4b displays the theoretical Taylor frequency, f_{th}, as a function of the experimental Taylor flow frequency f_T either upstream the porous medium (black and white triangles) or in the empty channel (gray stars). The data roughly collapse on a single trend (dashed line). Therefore, in spite of a noticeable impact on the bubble length (Fig. 4a), the presence of the porous medium does not affect significantly the Taylor flow frequency re-

spect to empty channel experiments. We observe that the global trend does not correspond to the slope 1. This can be explained by the crude approximations which lead to Eq. (5). First, due to the presence of gutters, the flow velocity in square cross-section channels is expected to be higher than $(Q_G + Q_L)/h^2$. Then, the liquid slug length may differ from $l_B Q_G/Q_L$ (Eq. (1)), leading to a nonlinear correction to Eq. (5). Finally, we neglected the lubrication films, while the cross-section liquid fraction may be up to $W = 20\%$ (see above).

The above results show that (1) at first order, the presence of the porous medium does not modify drastically the expected Taylor frequency upstream; (2) neither the bubble length nor the Taylor frequency exhibit a drastic change when the gas-liquid flow-rate ratio increases, in spite of the sudden change of hydrodynamic regime at the entrance of the porous medium. The regime transition between the Taylor-like regime and the modulated regime (Section 2.3) is therefore not due to a possible feedback of the flow in the foam on the upstream flow, but rather to the hydrodynamics and flow propagation *inside* the porous medium.

3.2. Dimensionless analysis

To quantify the hydrodynamic regimes, Serres et al. (2016) introduce a dimensionless number representative of the multiphase flow. Upstream the porous medium, the governing parameters are the flow-rate ratio, Q_G/Q_L, and the inertial and viscous forces, leading to the dimensionless number $Re_G/Re_L = (Q_G/Q_L)(\rho_G \mu_L/\rho_L \mu_G)$. Inside the porous medium, the dominant parameters are the velocity (typically $Q_G + Q_L$), the inertial and capillary forces, which define a multiphase Weber number $We = \rho_L(Q_G + Q_L)^2 d_w/(S^2 \sigma)$ where S is a typical surface through which the gas-liquid flow can propagate in a cross-section of the porous medium, and d_w the window diameter, representative of the pore structure for the flow. Following previous studies (Clements and Schmidt, 1980; Serres et al., 2016), a *modified* Weber number, We', accounting for both the hydrodynamics in the porous medium and the upstream flow, can be written:

$$We' = \left(\frac{\rho_G}{\sigma} \right) \left(\frac{\mu_L}{\mu_G} \right) \left(\frac{Q_G}{Q_L} \right) \left(\frac{Q_G + Q_L}{S} \right)^2 d_w . \qquad (6)$$

Here we also introduce the dimensionless frequency, also called the Strouhal number, defined by $St = f_0/(U/\lambda)$, where f_0 is the main frequency of the flow (see Section 2.2), $U = (Q_G + Q_L)/h^2$ the theoretical flow velocity and λ is given by Eq. (1), where l_B is taken as the experimentally measured bubble length.

Fig. 5 displays the Strouhal number versus the modified Weber number upstream the porous medium (white squares) and when entering the porous medium (gray circles). The data are the same than in Fig. 8 of Serres et al. (2016), but displayed with dimensionless parameters on both axes.

The two hydrodynamic regimes described in Section 2.3 are clearly visible: for $We' < 1$, the flow main frequency in the porous medium is conserved at the porous medium entrance; for $We' > 1$, the low frequency characteristics of the modulated regime appears. This result, already pointed out by Serres et al. (2016), was previously interpreted in terms of bubble fragmentation at the foam entrance. Indeed, the authors proposed that a critical bubble length l_B^* exists. For $l_B < l_B^*$, the incoming bubble from the Taylor flow can enter the porous medium and propagates as a whole; for $l_B > l_B^*$, a fragmentation mechanism was proposed, leading to the flow disorganization.

3.3. Experimental observations

To check the above hypothesis proposed by Serres et al. (2016), we performed additional experiments with a fast camera (see
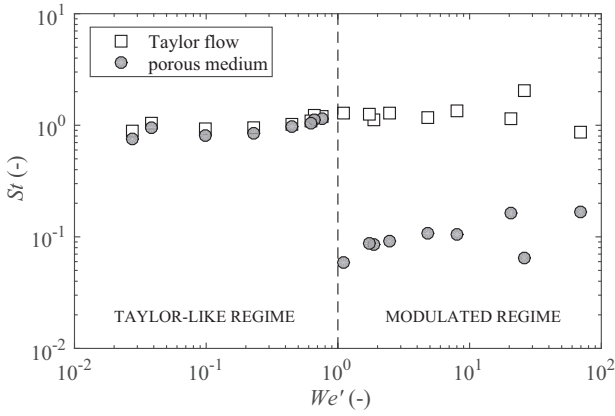
Fig. 5. Strouhal number, St, as a function of the modified Weber number, We' (see text) [white squares, Taylor flow upstream; gray circles, inside the porous medium]. The dashed line indicates the separation between the Taylor-like and the modulated regimes.

Section 2.1). High-speed imaging made it possible to have more information on the mechanism at the origin of the regime transition through direct visualization of the gas-liquid flow. The observations evidence that the mechanism at stake is not bubble fragmentation, but *coalescence*. Indeed, bubbles in the Taylor-like regime cross the porous medium as a whole, although deformed by their propagation in the solid foam (see Supplemental Material, movie 1). In the modulated regime, periodic bubbles crossing the medium alternate with a sudden bubble coalescence, which leads to the formation of a gas channel along the porous medium (see Supplemental Material, movie 2). This channel remains open for a certain time, then destabilizes and pinches off, leading back to the periodic bubbling regime.

Based on these observations we propose, in the next section, a phenomenological model to account for this mechanism. This model is then compared to experimental observations, with the final goal to predict the observed hydrodynamic regimes.

4. Phenomenological model

4.1. Description and hypotheses

The phenomenological model is based on the observations of bubble deformation when entering the porous medium. Taylor bubbles propagating in the millichannel upstream (length l_B^0, wavelength λ^0) are forced to propagate inside the porous medium through a smaller cross-section, typically of the cell size (diameter $a = d_c$, area $A = \pi a^2/4$) (Fig. 6a). Therefore, they are elongated (length l_B, wavelength λ) and we consider that the remaining cross-section area ($h^2 - A$) is occupied by the liquid phase only. The flow inside the porous medium is thus separated in two different zones, which can propagate *a priori* at different velocities: the gas-liquid zone (zone A, velocity u_A) and the pure liquid region (zone B, velocity u_B). This velocity difference, also called 'slip velocity' or 'drift flux', is classical and has already been pointed out in the literature (Wallis, 1969; Darton and Harrison, 1975; Larachi et al., 1991; Molga and Westerterp, 1997).

Assuming that the gas and liquid are incompressible, their flow rates in zone A can be written, respectively: $Q_G^A = Q_G = V_G u_A/\lambda$ and $Q_L^A = V_L^A u_A/\lambda$, where V_G is the volume of a gas bubble and V_L^A the volume of the liquid slug in zone A. The liquid flow rates in zones A and B can thus be written $Q_L^A = (V_L^A/V_G)Q_G = (\lambda/l_B - 1)Q_G$ and $Q_L^B = Q_L - Q_L^A$, respectively. The velocities of regions A and B are

then given by $u_A = (Q_L^A + Q_G)/A$ and $u_B = Q_L^B/(h^2 - A)$, leading to

$$u_A = \left(\frac{\lambda}{l_B}\right)\frac{Q_G}{A} \tag{7}$$

$$u_B = \frac{Q_L - (\lambda/l_B - 1)Q_G}{h^2 - A} \tag{8}$$

Note that $h > A$ and $\lambda \geq l_B$, so $u_A > u_B$ is always checked.

The second hypothesis of the model is that due to viscous losses, $u_A \to u_B$ with a relaxation time τ. At first order, one can assume an exponential relaxation:

$$\frac{\mathrm{d}u_a}{\mathrm{d}t} + \frac{u_a}{\tau} = u_B \tag{9}$$

with the initial condition $u_A = u_A^0$, leading to

$$u_A = (u_A^0 - u_B)\, \mathrm{e}^{-t/\tau} + u_B. \tag{10}$$

Replacing u_A and u_B by their expression given in Eqs. (7) and (8) provides the equation describing l_B normalized by the wavelength $\lambda(t)$:

$$\frac{l_B}{\lambda(t)} = \frac{\left(\frac{h^2}{A} - \mathrm{e}^{-t/\tau}\right)Q_G}{\left(\frac{h^2 - A}{A}\right)\left(\frac{\lambda^0}{l_B^0}\right)Q_G\, \mathrm{e}^{-t/\tau} + (Q_G + Q_L)(1 - \mathrm{e}^{-t/\tau})}. \tag{11}$$

Note that the bubble length is constant once it enters the porous medium, and given by $l_B = l_B^0 \times h^2/A$.

4.2. Relaxation time

A first estimation of the relaxation time τ can be obtained by considering that, in the modulated regime, the typical time at which coalescence occurs ($l_B = \lambda$) is given by $t = t_c \simeq 1/f_0$. This makes it possible to plot, from Eq. (11), the dependence of τ as a function of Q_L and Q_G (Fig. 7a). We find that τ decreases strongly with the liquid flow rate (Fig. 7a), while is does not depend drastically on the gas flow rate (Fig. 7a, inset).

However, to get a prediction on $l_B/\lambda(t)$ from the phenomenological model, it is necessary to estimate the relaxation time τ independently from Eq. (11). To do so, we assume that the liquid is the main responsible for viscous losses and relaxation and propose the following scaling, hereafter named τ_s. The relaxation time should be proportionnal to the liquid residence time in the foam, i.e. the typical time necessary for the liquid to cross the entire porous medium, $\tau_s \propto Lh^2/Q_L$. Moreover, when the liquid Reynolds number increases, the dissipation increases and the relaxation time decreases, so $\tau_s \propto Re_L^{-1}$, with $Re_L = \rho_L Ua/\mu_L$, $U = U_{TP} = (Q_G + Q_L)/h^2$ the two-phase flow characteristic velocity and $L = 16$ cm the total length of the porous medium. The scaling therefore gives $\tau_s \sim Re_L^{-1}(Lh^2/Q_L)$ and can be written

$$\tau_s \sim \frac{Lh^4\mu_L}{\rho_L(Q_G + Q_L)Q_L a}. \tag{12}$$

Note that τ_s only depends on the liquid properties (μ_L, ρ_L), as it is assumed that the relaxation through viscous losses is due mainly to the liquid phase.

Fig. 7b displays the relaxation time τ estimated from Eq. (11) with $t = 1/f_0$ as a function of the relaxation time τ_s predicted from this scaling. We find a fair proportionality, with a coefficient $\zeta \sim 20$ which cannot be determined by the dimensionless analysis (dashed line, Fig. 7b). The coefficient ζ must be interpreted with caution, due to the poor fitting in Fig. 7b. However, this simple phenomenological model only aims at predicting at first order the coalescence phenomenon, and the roughly linear
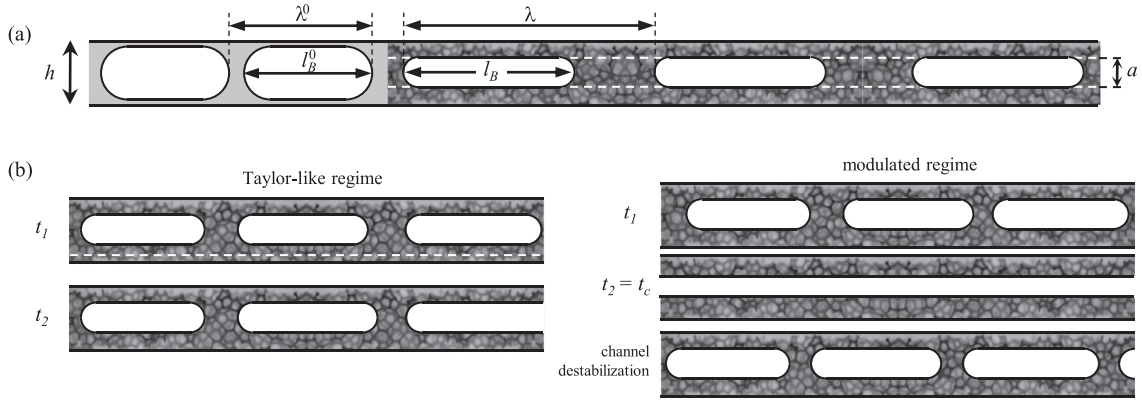
Fig. 6. (a) Sketch of the phenomenological model. Taylor bubbles (length l_B^0, wavelength λ^0) in the millichannel deform when entering the porous medium (length l_B, wavelength λ). They are forced to propagate in a narrower section, roughly corresponding to the pore section $A = \pi a^2/4$, where a is the pore diameter. (b) Two different regimes when the bubbles cross the porous medium. *Left:* The bubble deformation is small and they keep their periodicity – hence, the Taylor frequency – when propagating inside the porous medium. *Right:* The bubbles get closer and experience a coalescence inside the porous medium, leading to the formation of a gas channel (middle) after a typical time t_c. This channel then destabilizes, leading back to pediodic bubbles. This alternance generates a low-frequency (modulation) in the spatiotemporal evolution of ϵ_L.
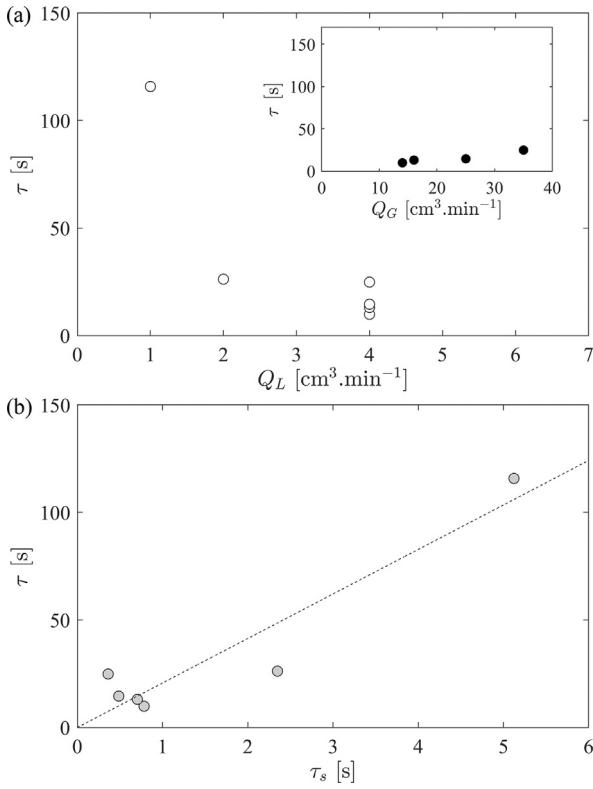

Fig. 7. (a) Relaxation time τ as a function of the liquid flow rate Q_L (main graph) and the gas flow rate Q_G (*Inset*). (b) Relaxation time τ determined from Eq. (11) as a function of τ_s determined from the scaling (Eq. (13)). The dashed line represents the linear fit (slope $\zeta \sim 20$).

trend in Fig. 7b is sufficient to provide an estimation of the relaxation time:

$$\tau_s = \frac{\zeta L h^4 \mu_L}{\rho_L (Q_G + Q_L) Q_L a} \qquad (13)$$

This estimation is independent from Eq. (11), knowing the parameters of the problem (cell geometry, porous structure, fluid properties and imposed gas and liquid flow rates).

4.3. Residence time

A second important time in the system is the residence time, t_s, corresponding to the typical time necessary for the bubbles to cross the entire porous medium. Indeed, as they cross the porous medium, the bubbles keep their length l_B constant, while the wavelength λ decreases (Eq. (11)). If $l_B \simeq \lambda$ for $t \leq t_s$, then the coalescence can occur, starting from the downstream end of the porous medium. This mechanism has been observed in the experiments with the fast camera.

The residence time of the gas phase is estimated by the equation :

$$t_s = \frac{(\epsilon - \epsilon_L) L h^2}{Q_G} \qquad (14)$$

where $(\epsilon - \epsilon_L) L h^2$ is the volume faction of the millichannel occupied by the gas phase, with ϵ the porosity and ϵ_L the liquid fraction estimated by direct visualization (Section 2.2).

4.4. Results

Fig. 8 displays the normalized bubble length, $l_B/\lambda(t)$, as a function of the time normalized by the residence time, t/t_s, when varying the liquid flow rate at constant gas flow rate (Fig. 8a) and when varying the gas flow rate at constant liquid flow rate (Fig. 8b). The bubble length l_B is computed from Eq. (11) by using the independent estimation of the relaxation time τ_s (Eq. (13)), and $a = d_c$ (the bubbles occupy typically a single cell in the channel cross-section). $l_B/\lambda(t)$ increases in time. If it reaches $l_B/\lambda = 1$ for $t < t_s$, i.e. before the gas has let the porous medium, then a coalescence should occur and the modulated regime should be observed. Otherwise, if $l_B/\lambda < 1$ for $t = t_s$, the model predicts that the bubbles manage to cross the entire porous medium without experiencing coalescence. The solid lines represent the sets of parameters for which a Taylor-like regime was observed, while the dashed lines indicate a modulated regime in the experiments. The phenomenological model is in good agreement with the experimental observations. It only fails to predict the hydrodynamic regimes for two sets of parameters (Q_G, Q_L) (Fig. 8): (10,1) and (10,2) Ncm^3 min^{-1}, for which the flow is close to the transition between both regimes.

Observations with the high speed camera point out, however, that in most cases, the bubbles occupy more than a single cell in the cross-section of the porous medium. The typical cell di-
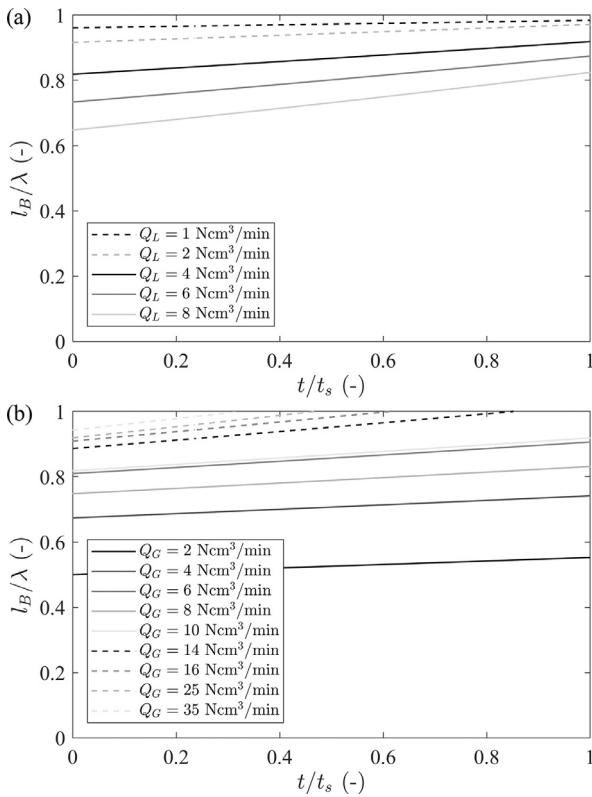
Fig. 8. Bubble length l_B normalized by the wavelength $\lambda(t)$ (computed from Eq. (11) with $a = d_c$) as a function of the time t normalized by the residence time t_s (a) for different liquid flow rates at constant gas flow rate [$Q_G = 10$ Ncm^3 min^{-1}]; (b) for different gas flow rates at constant liquid flow rate [$Q_L = 10$ Ncm^3 min^{-1}]. The solid or dashed lines represent the hydrodynamic regimes reported in the experiment: Taylor-like (solid lines) or modulated (dashed lines). The model fails in determining the hydrodynamic regimes for two sets of parameters (dashed lines in (a)).

Fig. 9. Bubble length l_B normalized by the wavelength $\lambda(t)$ (computed from Eq. (11) with $a = 3d_c$) as a function of the time t normalized by the residence time t_s (a) for different liquid flow rates at constant gas flow rate [$Q_G = 10$ Ncm^3 min^{-1}]; (b) for different gas flow rates at constant liquid flow rate [$Q_L = 10$ Ncm^3 min^{-1}]. The solid or dashed lines represent the hydrodynamic regimes reported in the experiment: Taylor-like (solid lines) or modulated (dashed lines). The model successfully predicts the hydrodynamic regimes.

ameter, $d_c = 604 \pm 86$ μm (see Section 2.1) is such that about 3 cells occupy the whole channel width. We then computed the normalized bubble length from the model, as described above, for $a = 3d_c$ ((Fig. 9). The model predicts successfully the hydrodynamic regimes reported in the experiments, including the two sets of parameters which were at the transition between both regimes (dashed lines in Figs. 8a and 9 a).

5. Conclusion

Based on the work of Serres et al. (2016), we proposed a phenomenological model to account for the two hydrodynamic regimes observed when a Taylor flow crosses a confined highly porous medium – here, an open cell solid foam of 96% porosity. We have shown that the tentative explanation of bubble fragmentation at the entrance, proposed in a previous work (Serres et al., 2016) is not corroborated by observations with a fast camera, which rather show bubble coalescence inside the medium. A simple phenomenological model based on neighboring bubbles getting closer to each other due to (1) the narrower section in which it is forced to enter the porous medium (pore vs. millichannel section) and (2) the evolution of the wavelength in time during propagation along the medium recovers, at first order, the two hydrodynamic regimes. On the one hand, if the bubbles do not get close enough before exiting the porous medium, the frequency in the open cell
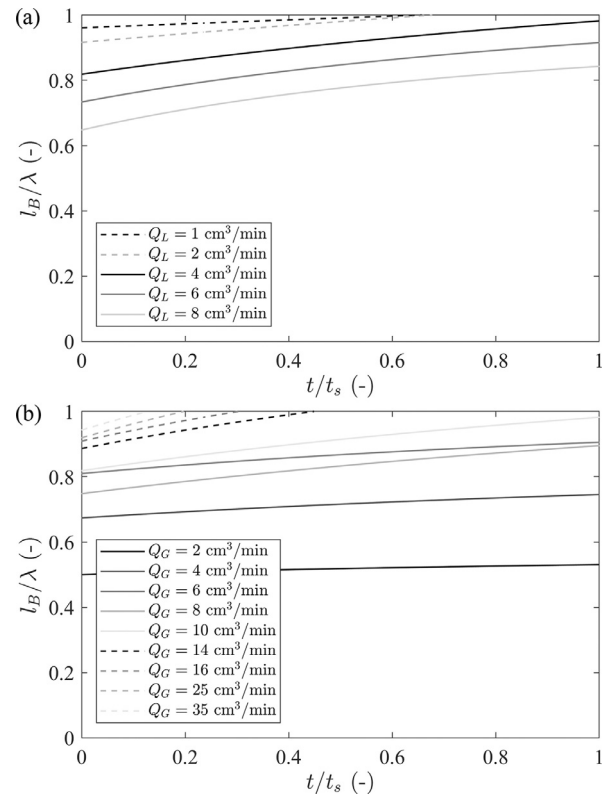
solid foam remains equal to the Taylor frequency at the entrance (Taylor-like regime). On the other hand, when the wavelength decreases enough to connect bubbles, a coalescence is reported, leading to the formation of a channel along the medium. A continuous degassing through the foam then occurs. The channel further destabilizes, leading back to periodic bubbles. This introduces a low frequency in the system, corresponding to the modulated regime.

Although this first order model captures well the observations, further improvements could be made. In particular, one could account for a more realistic bubble volume, including the meniscii volume computation and a bubble length variation during its propagation. In addition, the proposed model does not depend explicitly neither on the gas properties nor on surface tension, which may impact the bubble coalescence mechanism. This parameter is hidden in the factor ζ (Eq. (13)), which has to be adjusted from the relaxation time estimation (Fig. 7b). Changing the surface tension and investigating the empirical dependence of ζ on this parameter could be the goal of a future work.

Supplementary material

Supplementary material associated with this article can be found, in the online version, at 10.1016/j.ijmultiphaseflow.2018.04.003.

References

Abadie, T., Aubin, J., Legendre, D., Xuereb, C., 2012. Hydrodynamics of gas-liquid taylor flow in rectangular microchannels. Microfluid. Nanofluid. 12, 355–369.

Angeli, P., Gavriilidis, A., 2008. Taylor flow in microchannels. In: Li, D. (Ed.), Encyclopedia of Microfluidics and Nanofluidics. Springer, US, pp. 1971–1976.

Aussillous, P., Quéré, D., 2000. Quick deposition of a fluid on the wall of a tube. Phys. Fluids 12, 2367–2371.

Babchin, A., Brailovsky, I., Gordon, P., Sivashinsky, G., 2008. Fingering instability in immiscible displacement. Phys. Rev. E 77. 026301

Clements, L.D., Schmidt, P.C., 1980. Dynamic liquid holdup in two-phase downflow in packed beds: air-silicone oil system. AIChE J. 26 (2), 317–319.

Darton, R.C., Harrison, D., 1975. Gas and liquid holdup in three-phase fluidisation. Chem. Eng. Sci. 30, 581–586.

Dittmar, D., Fredenhagen, A., Oei, S.B., Eggers, R., 2003. Interfacial tensions of ethanolcarbon dioxide and ethanolnitrogen. dependence of the interfacial tension on the fluid density–prerequisites and physical reasoning. Chem. Eng. Sci. 58, 1223–1233.

Eccles, J.K., Pratson, L., Newell, R.G., Jackson, R.B., 2009. Physical and economical potential of geological CO_2 storage in saline aquifers. Environ. Sci. Technol. 43, 1962–1969.

Faridkhou, A., Larachi, F., 2012. Hydrodynamics of gas-liquid cocurrent flows in micropacked beds – wall visualization study. Ind. Eng. Chem. Res. 51, 16495–16504.

Garstecki, P., Fuerstman, M.J., Stone, H.A., Whitesides, G.M., 2006. Formation of droplets and bubbles in a microfluidic t-junction–scaling and mechanism of break-up. Lab Chip 6, 437–446.

Gay, A., Lopez, M., Cochonat, P., Sérane, M., Levaché, D., Sermondadaz, G., 2006. Isolated seafloor pockmarks linked to BSRs, fluid chimneys, polygonal faults and stacked oligocene miocene turbiditic palaeochannels in the lower congo basin. Mar. Geol. 226, 25–40.

Hessel, V., Angeli, P., Gavriilidis, A., Löwe, H., 2005. Gas-liquid and gas-liquid–solid microscructured reactors: contacting principles and applications. Ind. Eng. Chem. Res. 44, 9750–9769.

Hovland, M., Gardner, J.V., Judd, A.G., 2002. The significance of pockmarcks to understanding fluid flow processes and geohazards. Geofluids 2, 127–136.

Kang, Q., Tsimpanogiannis, I.N., Zhang, D., Lichtner, P.C., 2005. Numerical modeling of pore-scale phenomena during CO_2 sequestration in oceanic sediments. Fuel Process. Technol. 86, 1647–1665.

Kreutzer, M.T., Kapteijn, F., Moulijn, J.A., Heiszwolf, J.J., 2005. Multiphase monolith reactors: chemical reaction engineering of segmented flowin microchannels. Chem. Eng. Sci. 60, 5895–5916.

Lali, F., Pahner, F.A., Lange, R., 2016. Modeling and simulation of the hydrogenation of α-methylstyrene on catalytically active metal foams as tubular reactor packing. Int. J. Chem. Eng.. 782381

Larachi, F., Laurent, A., Wild, G., Midoux, N., 1991. Some experimental liquid saturation results in fixed-bed reactors operated under elevated pressure in cocurrent upflow and downflow of the gas and the liquid. Ind. Eng. Chem. Res. 30, 2404–2410.

Leclerc, A., Philippe, R., Houzelot, V., Schweich, D., de Bellefon, C., 2010. Gas-liquid taylor flow in square micro-channels: new inlet geometries and interfacial area tuning. Chem. Eng. J. 165, 290–300.

Losey, M.W., Schmidt, M.A., Jensen, K.F., 2001. Microfabricated multiphase packed-bed reactors: characterization of mass transfer and reactions. Ind. Eng. Chem. Res. 40, 2555–2562.

Marquez, N.P.C., Makkee, M., Moulijn, J.A., Kreutzer, M.T., 2008. Dispersion and holdup in multiphase packed bed microreactors. Chem. Eng. Technol. 31 (8), 1130–1139.

Mastalerz, V., de Lange, G.J., Dählmann, A., Feseker, T., 2007. Active venting at the isis mud volcano, offshore egypt: origin and migration of hydrocarbons. Chem. Geol. 246, 87–106.

Mazzini, A., Svensen, H., Akhmanov, G.G., Aloisi, G., Planke, S., Malthe-Sørenssen, A., Istadi, B., 2007. Triggering and dynamic evolution of the LUSI mud volcano, Indonesia. Earth Planet. Sci. Lett. 261, 375–388.

Molga, E.J., Westerterp, K.R., 1997. Experimental study of a cocurrent upflow packed bed bubble column reactor: pressure drop, holdup and interfacial area. Chem. Eng. Prog. 36, 489–495.

Naudts, L., Greinert, J., Artemov, Y., Beaubien, S.E., Borowski, C., De Batist, M., 2008. Anomalous sea-floor backscatter patterns in methane venting areas, dnepr paleo-delta, NW black sea. Mar. Geol. 251, 253–267.

Planke, S., Svensen, H., Hovland, M., Banks, D.A., Jamtveit, B., 2003. Mud and fluid migration in active mud volcanoes in azerbaijan. Geo-Mar. Lett. 23, 258–268.

Reddy, K.R., Adams, J.A., 2001. Effects of soil heterogeneity on airflow patterns and hydrocarbon removal during in situ air sparging. J. Geotech. Geoenviron. Eng. 3, 234–247.

Roudet, M., 2008. Hydrodynamique et Transfert de Masse Autour d'une Bulle Confinée Entre Deux Plaques. Institut National Polytechnique de Toulouse Ph.d. thesis. 131 p.

Semer, R., Adams, J.A., Reddy, K.R., 1998. An experimental investigation of air flow patterns in saturated soils during air sparging. Geotech. Geol. Eng. 16, 59–75.

Serres, M., Zanota, M.L., Philippe, R., Vidal, V., 2016. On the stability of Taylor bubbles inside a confined highly porous medium. Int. J. Multiphase Flow 85, 157–163.

Stemmet, C.P., Bartelds, F., van der Schaaf, J., Kuster, B.F.M., Schouten, J.C., 2008. Influence of liquid viscosity and surface tension on the gas-liquid mass transfer coefficient for solid foam packings in co-current two-phase flow. Chem. Eng. Res. Des. 86, 1094–1106.

Stemmet, C.P., Jongmans, J.N., van der Schaaf, J., Kuster, B.F.M., Schouten, J.C., 2005. Hydrodynamics of gas-liquid counter-current flow in solid foam packings. Chem. Eng. Sci. 60, 6422–6429.

Stemmet, C.P., van der Schaaf, J., Kuster, B.F.M., Schouten, J.C., 2006. Solid foam packings for multiphase reactors – modelling of liquid holdup and mass transfer. Chem. Eng. Res. Des. 84 (A10), 1134–1141.

Tourvielle, J.N., Philippe, R., de Bellefon, C., 2015a. Milli-channel with metal foams under an applied gas-liquid periodic flow: external mass transfer performance and pressure drop. Chem. Eng. J. 267, 332–346.

Tourvielle, J.N., Philippe, R., de Bellefon, C., 2015b. Milli-channel with metal foams under an applied gas-liquid periodic flow: flow patterns, residence time distribution and pulsing properties. Chem. Eng. Sci. 126, 406–426.

Twigg, M.V., Richardson, J.T., 2007. Fundamentals and applications of structured ceramic foam catalysts. Ind. Eng. Chem. Res. 46, 4166–4177.

van Steijn, V., Kreutzer, M.T., Kleijn, C.R., 2007. μ-PIV study of the formation of segmented flow in microfluidic t-junction. Chem. Eng. Sci. 62, 7505–7514.

Wallis, G.B., 1969. One-Dimensional Two-Phase Flow. McGraw Hill, New York.

Zapico, R.R., Marín, P., Díez, F.V., Ordóñez, S., 2016. Liquid hold-up and gas-liquid mass transfer in an alumina open-cell foam. Chem. Eng. Sci. 143, 297–304.